Proceedings of the 9ICEG
9th International Congress on Environmental Geotechnics
25-28 June, 2023 | Chania, Greece
© Authors: All rights reserved, 2023
https://doi.org/10.53243/ICEG2023-33

Molecular Forces of Water Flow in Clay Nanopores

Sheng-Jie Wei[1], Yu-Chao Li[2*], Peng Shen[3] and Yun-Min Chen[4]

[1]Ph.D. candidate, MOE Key Laboratory of Soft Soils and Geoenvironmental Engineering, College of Civil Engineering, Zhejiang University, Hangzhou, P. R. China, email: sheng-jie_wei@zju.edu.cn

[2]Professor, corresponding author, MOE Key Laboratory of Soft Soils and Geoenvironmental Engineering, College of Civil Engineering, Zhejiang University, Hangzhou, P. R. China, email: liyuchao@zju.edu.cn

[3]Ph.D. candidate, MOE Key Laboratory of Soft Soils and Geoenvironmental Engineering, College of Civil Engineering, Zhejiang University, Hangzhou, P. R. China, email: 12012046@zju.edu.cn

[4]Professor, MOE Key Laboratory of Soft Soils and Geoenvironmental Engineering, College of Civil Engineering, Zhejiang University, Hangzhou, P. R. China, email: chenyunmin@zju.edu.cn

ABSTRACT

Clays have complex multiscale pore structures and water flow in clay nanopores plays an important role in various engineering applications, such as adsorption of pollutants and barriers of contaminated lands. Therefore, the micro-physical mechanism is necessary to be considered from bottom up to better control the nanoscale water flow process and the computational simulation has become the main method to study the process. In this paper, non-equilibrium molecular dynamics (NEMD) simulations are performed to investigate the hydrodynamics properties and the molecular forces of water flow in montmorillonite nanopores. The velocity profiles of water flow are parabolic but slight offsets are observed near the surfaces. The simulated dynamic viscosity of water is 0.72±0.04 cP and the average hydraulic conductivities are (1.61±0.01), (3.05±0.07), and (5.21±0.33) $\times 10^{-11}$ m/s for pore size h = 3.5, 5.0, and 6.5 nm, respectively. During the NEMD simulations, the time-fluctuation of the force of clay matrix F^{sc} on the water molecules in clay nanopores is found to satisfy the Gaussian distribution and its time-average value basically equals the applied force F^{d} to maintain a dynamic mechanical equilibrium. The mechanical-equilibrium water flow can be equivalent as a simply supported beam with four distributed forces acting on it. The force of clay f^{s}, similar to the pedestal counter force, concentrates on the water molecules in the adsorbed layer while the force of cations f^{c} is mainly exerted on the diffuse layer. The integral of driving force f^{d}, the force of clay f^{s} and the force of cations f^{c} along the z-axis induce the shear strain of the pore water while the integral of the force of water molecules f^{w} can be regarded as the internal viscous force to resist the shear deformation.

Keywords: molecular dynamics, hydrodynamics, clay nanopore, molecular force, boundary effect

1 INTRODUCTION

Clays have complex multiscale pore structures (Boţan et al., 2011; Bourgh and Ajo-Franklin, 2017) and these structures act as significant passageways for the transport of mass. Water flow in the clay

nanopores, in particular, plays an important role in various engineering applications, such as seepage through soil/shale (Kristinanto & Rahardjo, 2018), remediation of contaminated lands (Torres et al., 2018) and oil exploitation (Fang et al., 2019). However, the classic Navier-Stokes equation seems questionable to describe the nanoscale water flow behaviors accurately (Sam et al., 2020) due to excessive molecular fluctuations and inhomogeneous hydrodynamics properties (Daivis & Todd, 2018). Therefore, the micro-physical mechanism is necessary to be considered from bottom up to better control the nanoscale water flow process and the computational simulation has become the main method to study the process.

With the progress of computer calculation capacity, molecular dynamics (MD) method was widely applied to investigate the diffusion behaviors (Ichikawa et al., 2002), viscosity (Yeh and Hummer, 2004) and morphologies (Cao et al., 2006) of the water molecules in clay nanopores, while the non-equilibrium molecular dynamics (NEMD) simulation had better performances for simulating water flows (Travis et al., 1997; Ramos-Alvarado et al., 2016). NEMD is able to provide a link between the microscopic level and the macroscopic level (Hoover & Hoover, 2005). A series of simulations were performed to determine the slip length of the water flow in clay nanopores and the simulated values were applied to modify the continuum model (Boţan et al., 2011). However, the deviations between the simulated velocities and the continuum model results near the mineral surface were still unable to be modified (Hansen et al., 2011). Further simulations demonstrated that the slip length could be better predicted by mineral contact angle, interfacial water structure and planar atomic density (Ramos-Alvarado et al., 2016). The influences of the salt concentration and ion specificity on the hydrodynamics in clay nanopores were also investigated by NEMD simulations, which showed that although the influences became comparatively indistinctive far from the mineral surface (Simonnin et al., 2018), the increase of salt concentration enhanced the hydrogen-bonding network of water and the viscosity of water linearly increased with salt concentrations (Yin & Zhao, 2020).

Nevertheless, few of them explored hydrodynamics of water flow in clay nanopores from the perspective of molecular forces. This paper performs NEMD simulations on the water flow processes in montmorillonite nanopores with three pore sizes under two different flow-driving pressures. The density profiles of water and cations are first illustrated to determine the flowing zones in clay nanopores. Subsequently, the flow velocities, slip lengths, water viscosity and hydraulic conductivities are calculated to assess the hydrodynamics properties of water flow in clay nanopores. Finally, the molecular forces of clay crystal layers and cations on the pore water are further analyzed.

2 MODELS AND METHODS

The Na-montmorillonite with unit formula of $Na_{0.75}Si_8[Al_{3.25}Mg_{0.75}]O_{20}(OH)_4$ is considered in this paper. A single crystal layer is composed of 32 (8×4) unit-cells and its planar size is 42.24 Å (L_x) × 36.56 Å (L_y) with a thickness d of 6.56 Å, as illustrated in Figure 1. Periodic boundary condition is applied to all three directions and an infinitely long flow path is formed in y-direction. To model the slit-like clay nanopores with various pore sizes, the clay layer is divided into two halves with three different separation distances h (i.e., pore size h = 3.5, 5.0, and 6.5 nm) in the z-direction. There is no doubt that the accessible width for water molecules h^* is smaller than h. In practice, h^* is assumed to be the distance between the first adsorbed water layers (Hansen et al., 2011; Kannam et al., 2013). Based on the mass density of bulk

water ρ_w = 0.997 g/cm^3, the number of water molecules N_w to fill in the nanopore is 1665, 2437 and 3209 for h = 3.5, 5.0 and 6.5 nm, respectively.

The clay matrix (including the clay crystal layers and cations) is described by CLAYFF force field (Cygan et al., 2004; Li et al., 2020) and the extended simple point charge (SPC/E) water model (Berendsen et al., 1981) is used to simulate the behaviors of water molecules. The cut-off distance 10 Å for Lennard-Jones interactions and Ewald summation with an accuracy of 0.0001 for the long-range electrostatic interactions are adopted. The open source package LAMMPS (Plimpton, 1995) is applied to perform the simulations and the software OVITO-basic (Stukowski, 2010) is utilized for visualization.

To simulate the water flow in the clay nanopores, a driving force f_w^d is applied to each water molecule in y-direction, which generates an identical acceleration a_y on each water molecule and a total driving force F^d (see Table 1 for used values in the simulations). The mobile atoms have a non-zero net velocity due to the extra artificial force applied to the water molecules in y-direction, which will generate unreasonable fictitious temperature. Therefore, the y-velocity of the center of mass of the water molecules is subtracted out during the thermostatic process in the NEMD simulations (Boţan et al., 2011). Under the applied flow-driving force, the NEMD simulation is performed for 2 ns to achieve a steady state. The trajectories and interaction forces of the particles are collected every 0.1 ps during the next 2 ns.

Table 1. *The used parameters for NEMD simulations.*

ΔP (MPa)	a_y (×10^{12} m/s^2)	f_w^d (×10^{-13} N)	F^d (×10^{-10} N)		
			h = 3.5 nm (N_w = 1665)	h = 5.0 nm (N_w = 2437)	h = 6.5 nm (N_w = 3209)
20	5.49	1.64	2.73	4.00	5.27
60	32.9	9.85	16.4	24.0	31.6

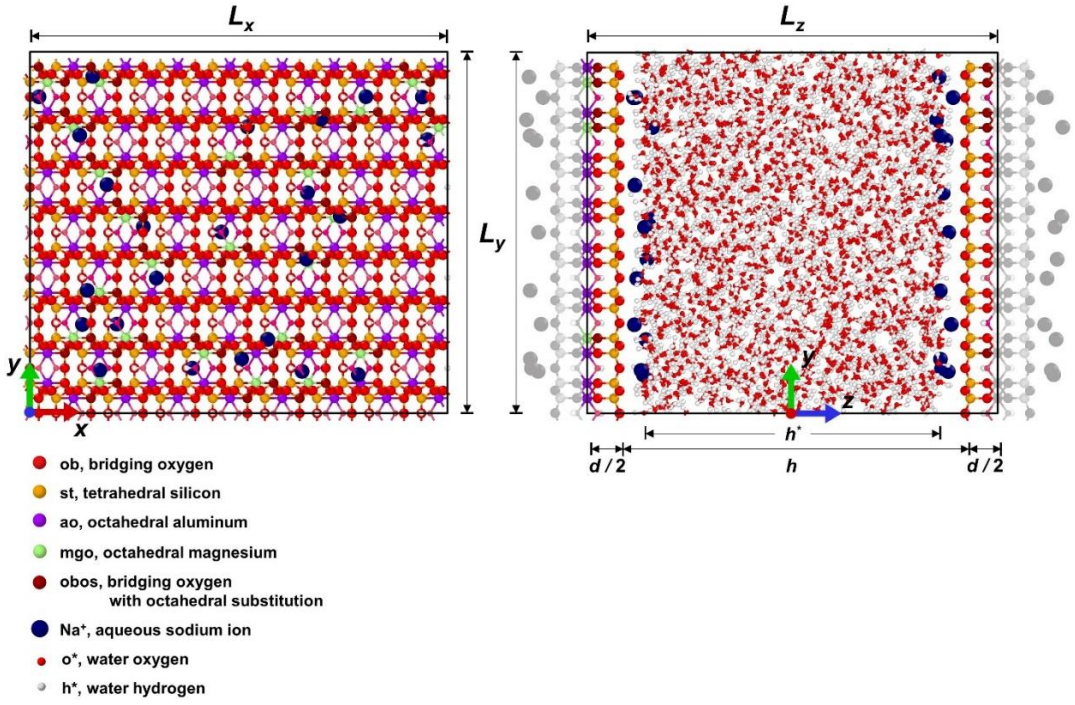

Figure 1. *Molecular model for Wyoming-montmorillonite nanopores.*

3 RESULTS AND DISCUSSIONS

3.1 Concentration Profile

The slit-like nanopore is equally divided into N_{bin} laminae along the *z*-direction and the width of each lamina is about 0.05 nm. The molar concentration of water oxygen, water hydrogen and Na^+ in each lamina was calculated. As illustrated in Figure 2, the clay nanopore can be divided into three zones, that is, the adsorbed layer, the diffuse layer and the bulk region.

The adsorbed layer starts from the clay mineral surfaces and its range has no significant change with various pore sizes. The width of the adsorbed layer (~0.35 nm) basically equals the diameter of a water molecule, indicating one single water layer is formed in the adsorbed layer. Those water molecules are highly orientational polarized with one of the water hydrogen atoms pointing towards the surface while the other one pointing away from the surface. The first concentration peak of water oxygen atom (0.25 ~ 0.30 nm from the clay mineral surface) shows the location of the first adsorbed water layer. The concentration of Na^+ in the adsorbed layer is extremely low, which implies the inner-sphere complex of Na^+ (that is, cations binding directly to the surface without intervening water molecules) is hard to form when the substitution sites are not at the tetrahedral sheet.

The diffuse layer follows after the adsorbed layer and ends as the concentration of various pore solution particles remain stable. According to the Electric Double Layer theory (Mitchell and Soga, 2005), the width of the diffuse layer is inversely proportional to the concentration of pore solution. Hence, other things being the same, the range of the diffuse layer enlarges with the increase of pore size (0.90, 1.15 and 1.85 nm for h = 3.5, 5.0 and 6.5 nm respectively). In the diffuse layer, the hydrated Na^+ tend to form the outer-sphere complex (that is, attaching to the surface with its hydration sphere) and an evident peak of concentration occurs. Subsequently, the concentration of Na^+ decays smoothly while the concentration of water molecules goes through two slight oscillations. The water molecules in the diffuse layer gradually transit from the ordered polarization state to the disordered bulk sate.

In the bulk region, the concentration of water hydrogen atoms and oxygen atoms basically maintain constant, and the concentration of Na^+ almost decays to zero. Therefore, the fluid in this region can be regarded as free bulk water.

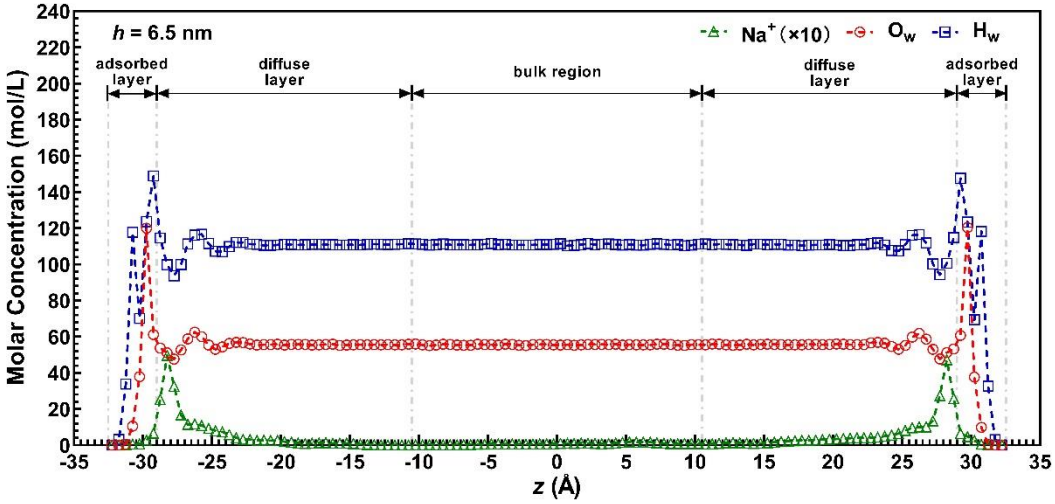

Figure 2. *Molar concentration of water oxygen atoms, hydrogen atoms and Na^+ for h = 6.5 nm.*

3.2 Hydrodynamics Properties

Based on the bin method (Liu et al., 2018), the velocity profiles in various sizes of clay nanopores under different flow-driving pressures are illustrated in Figure 3. The vertical dashed lines represent the locations of the surface oxygen atoms of the clay crystal layers and the dot-dashed lines represent the first adsorbed layers of water molecules.

If the density and viscosity of the confined water are uniform and homogeneous, the velocity profile is assumed to be parabolic (Poiseuille flow) according to Navier-Stokes equation (Travis et al., 1997; Hansen et al., 2011). It is clear that the flow velocity of water molecules between the first adsorbed water layers can be well fit by the parabolic function but slight offsets can also be observed near the mineral surfaces. Those offsets result from the discreteness of the water at the vicinity of clay surface, which are unable to be described by the Navier-Stokes equation.

The parabolic part of the velocity profile can be expressed by Equation (1):

$$v_y(z) = -\frac{1}{2\mu}\frac{\Delta P}{L_y}\left[z^2 - \left(\frac{h^*}{2}\right)^2 - l_s \cdot h^*\right] \tag{1}$$

where μ is the dynamic viscosity of water and l_s is the slip length. Fitting the parabolic part of the velocity profiles by Equation (1) and the values of μ and l_s can be obtained, as listed in Table 2. Obviously, the dynamic viscosity of water μ maintains stable for various pore sizes and equivalent flow-driving pressure. The obtained value of μ = 0.72±0.04 cP is close to the value of water viscosity (0.64±0.01 cP) obtained by other researchers using the same SPC/E water model (Hess, 2002). All values of l_s are greater than zero indicating a slip boundary and the l_s for water flow in the clay nanopores increases with ΔP.

Given that the flow velocity dramatically decreases to zero in the adsorbed water layers, the mean flow velocity obtained by averaging the velocity profiles between two adsorbed water layers is close to that obtained by averaging the whole velocity profiles, and the relative error is less than 6%. As the velocity

profiles between two adsorbed water layers follow the Navier-Stokes Equation, it is reasonable to calculate the hydraulic conductivity $\bar{k}$ via the Darcy's Law based on the former mean flow velocity $\bar{v}$, as shown in Table 2. It is noted that the obtained values of $\bar{k}$ vary with h but basically do not change with ΔP. The average hydraulic conductivities are (1.61±0.01), (3.05±0.07), and (5.21±0.33) $\times 10^{-11}$ m/s for h = 3.5, 5.0, and 6.5 nm, respectively. Those values have the same order of magnitudes with the results obtained by laboratory experiments for montmorillonites (Shackelford, 2005; Katsumi et al., 2015).

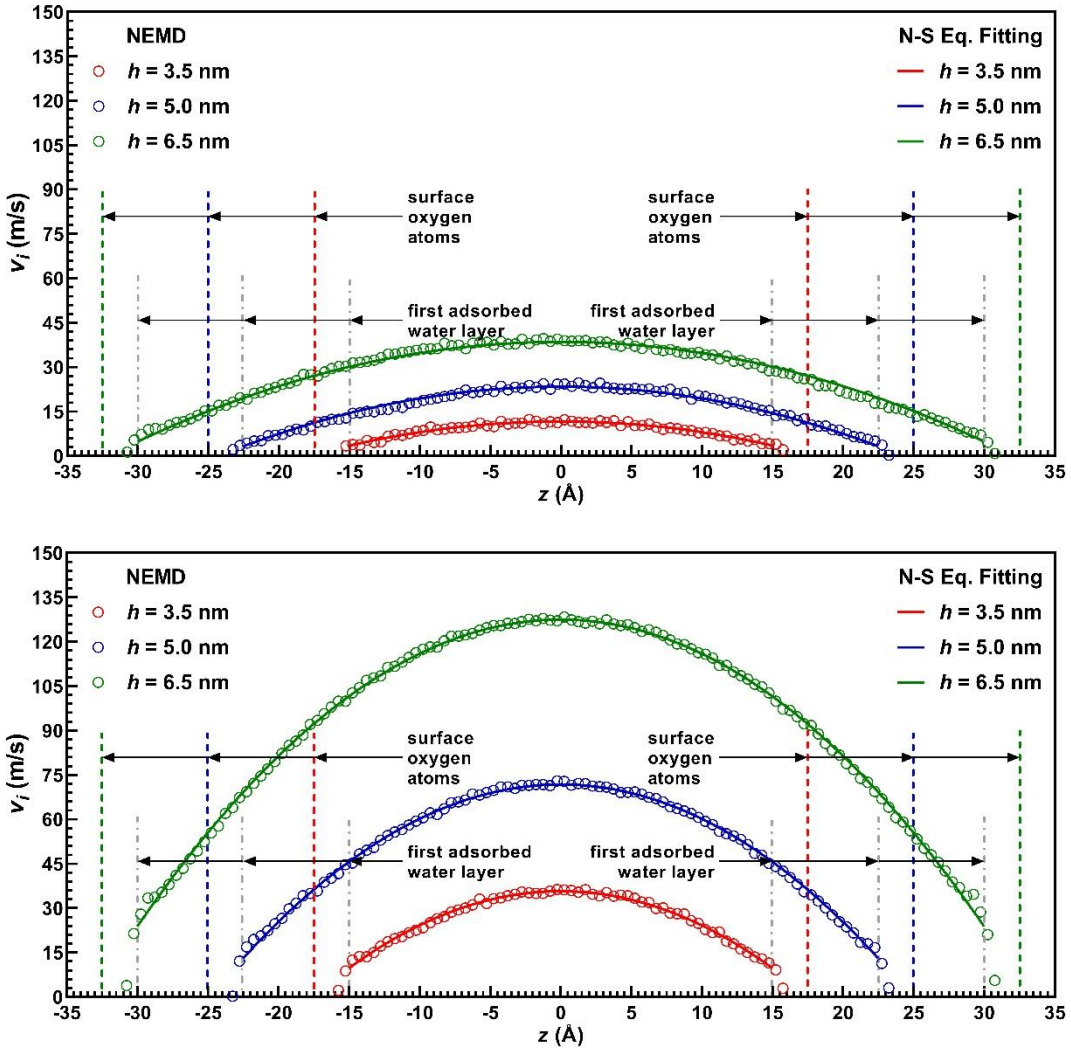

Figure 3. *Velocity profiles in clay nanopores. ΔP = 20 MPa (upper) and ΔP = 60 MPa (lower).*

Table 2. *Hydrodynamics properties of water flow in clay nanopores.*

***pore size h* (nm)**	***driving pressure ΔP* (MPa)**	***dynamic viscosity μ* (cP)**	***slip length l_s* (nm)**	**mean flow velocity $\bar{v}$ (m/s)**	**average hydraulic conductivity $\bar{k}$ ($\times 10^{-11}$ m/s)**
3.5	20	0.76	0.22	8.9	1.60
	60	0.71	0.28	27.1	1.61
5.0	20	0.69	0.18	16.7	2.98
	60	0.71	0.25	52.2	3.11
6.5	20	0.73	0.22	27.3	4.88
	60	0.71	0.35	93.0	5.54

3.3 Molecular Forces

In this section, the molecular forces on pore water are investigated to provide a new insight into the mechanisms of the boundary effect in the vicinity of clay mineral surfaces and the viscosity of water. It is noted that only the molecular forces along the flow direction (i.e., the *y*-direction) are considered below. A positive force indicates that the direction of the force is the same as the flow direction (i.e., a driving force to the water flow); on the contrary, a negative force indicates that the direction of the force is opposite to the flow direction (i.e., a resistant force to the water flow).

The total force of clay crystal layers (annotated as 's') and cations (annotated as 'c') on the pore water F^{sc} is collected every 0.1 ps during the 2 ns sampling period. According to the obtained data, it is clear that F^{sc} are fluctuant within a great range during the sampling time rather than keeping constant even after the system has achieved the thermodynamic equilibrium state and the time-fluctuation of F^{sc} satisfies the Gaussian distribution. The differences between the absolute time-averaged values of F^{sc} and the corresponding F^{d} (see Table 1) are 4.7×10^{-11} and 9.0×10^{-12} N and the relative errors are 17.2% and 0.5% for ΔP = 20 and 60 MPa, respectively. Hence, the time-average values of F^{sc} basically equal to F^{sc} and the confined pore water maintain a dynamic mechanical equilibrium during the NEMD simulations.

Further analyses of molecular forces on water molecules in clay nanopores are conducted. There are four distributed forces acting on water molecules in each water lamina, that is, the flow-driving force (f^{d}), the force of clay crystal layers (f^{s}), the force of cations in nanopores (f^{c}) and the force of water molecules in other laminae (f^{w}). The profile of these forces along the *z*-axis under ΔP = 60 MPa is taken as an example and plotted in Figure 4. Obviously, the variations of these forces are highly correlated to the concentration profile of water molecules and Na^{+} (see Figure 2). The artificial driving force f^{d} (red curve in Figure 4) is proportional to the concentration of water molecules. The force from the clay crystal layers f^{s} (orange curve in Figure 4), similar to the pedestal counter force, is a resistant force (i.e., $f^{s} < 0$) concentrating on the water molecules in the adsorbed layer, with a peak value of about -3.56 (-3.63) N/m. It transforms to be a driving force (i.e., $f^{s} > 0$) in the diffuse layer and gradually decays to zero. Being different from f^{s}, the force from the compensating cations f^{c} (green curve in Figure 4) chiefly concentrates on the water molecules in the diffuse layer. At the range of 0.35 ~ 0.50 nm from the clay surface, the Na^{+} and surrounding water molecules form the outer-sphere complex due to ion hydration (Figure 2) and thus the cations exert a driving force (i.e., $f^{c} > 0$) to the surrounding water molecules. Subsequently, as the further diffusion of Na^{+} takes place, f^{c} turns to be a resistant force and its value gradually decays to near zero after a transitory increment. The force from the water molecules in other water laminae f^{w} (blue curve in Figure 4) serves as a driving force in the adsorbed layer and transforms to be a resistant force in the diffuse layer as well as the bulk region. Water molecules in the laminar flow are at a state of dynamic mechanical equilibrium, therefore, each water lamina can be equivalent as a simply supported beam under the distributed loads of f^{d}, f^{s}, f^{c} and f^{w}, as illustrated in Figure 4. As for the pore water, to some extent, the integral of f^{d}, f^{s} and f^{c} along the *z*-axis induce motion and shear strain while the integral of f^{w} serves as the internal viscous force within the pore water to resist the shear deformation.

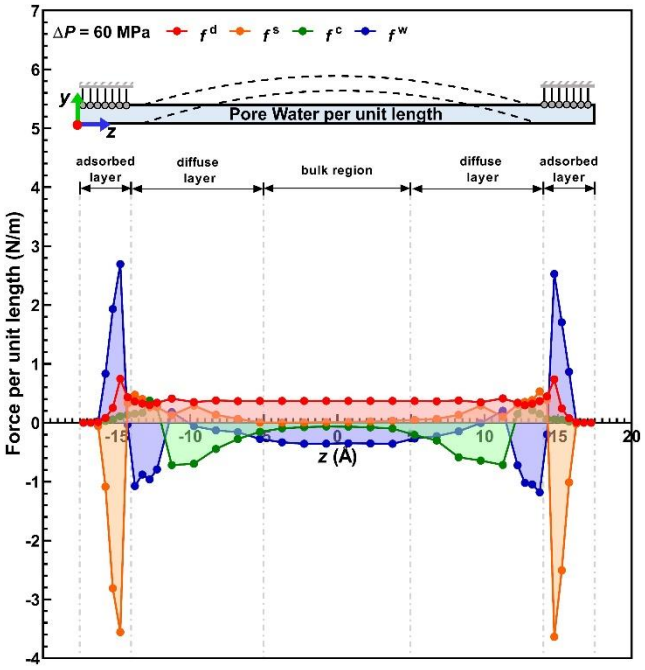

Figure 4. *Profile of forces on water molecules in each water lamina under ΔP = 60 MPa.*

4 CONCLUSIONS

In this paper, the water flow in the nanopores of Na-montmorillonite is simulated by the NEMD simulations. The hydrodynamics properties are quantitatively investigated and the molecular forces on the pore water are calculated. The following conclusions can be drawn:

(1) According to the distribution characteristic of cations and water molecules, the clay nanopore can be divided into the adsorbed layer, the diffuse layer and the bulk region. The width of the adsorbed layer basically equals the diameter of a single water molecule and those water molecules are highly orientational polarized. In the diffuse layer, the width enlarges with the increase of pore size (0.90, 1.15 and 1.85 nm for h = 3.5, 5.0, and 6.5 nm respectively) and the hydrated Na^+ tend to form the outer-sphere complex.

(2) The velocity profiles of water flow are parabolic but slight offsets can be observed near the surfaces. The simulated dynamic viscosity of water is 0.72±0.04 cP. The values of l_s indicate a slip boundary and it increases with ΔP. The average hydraulic conductivities are (1.61±0.01), (3.05±0.07), and (5.21±0.33) $\times 10^{-11}$ m/s for pore size h = 3.5, 5.0, and 6.5 nm, respectively.

(3) The time-fluctuation of F^{sc} satisfies the Gaussian distribution and the time-average values of F^{sc} basically equal to F^{sc} to maintain a dynamic mechanical equilibrium of confined pore water. The mechanical-equilibrium water flow can be equivalent as a simply supported beam with four distributed forces acting on it. The f^s, similar to the pedestal counter force, concentrates on the water molecules in the adsorbed layer, while the f^c is mainly exerted on the diffuse layer. The f^w serves as the internal viscous force within the pore water to resist the shear deformation.

5 ACKNOWLEDGEMENTS

The financial supports received from the National Natural Science Foundation of China (NSFC, Grant No. 51988101, 42077241 and 42277125) and the National Key R&D Program of China (Grant No. 2019YFC1806002) are gratefully acknowledged. We thank Hangjun Wu in the Center of Cryo-Electron Microscopy (CCEM), Zhejiang University for his technical assistance on providing the computational resources.

REFERENCES

Boţan, A., Rotenberg, B., Marry, V., Turq, P., & Noetinger, B. (2011). Hydrodynamics in Clay Nanopores. The Journal of Physical Chemistry C, 115, 16109-16115.

Bourg, I. C., & Ajo-Franklin, J. B. (2017). Clay, Water, and Salt: Controls on the Permeability of Fine-Grained Sedimentary Rocks. Accounts of Chemical Research, 50, 2067-2074.

Cao, B. Y., Chen, M., & Guo, Z. Y. (2006). Liquid Flow in Surface-Nanostructured Channels Studied by Molecular Dynamics Simulation. Physical Review E: Statistical Nonlinear Soft Matter Physical, 74, 066311.

Cygan, R. T., Liang, J.-J., & Kalinichev, A. G. (2004). Molecular Models of Hydroxide, Oxydroxide, and Clay Phases and the Development of a General Force Field. The Journal of Physical Chemistry B, 108, 1255-1266.

Daivis, P., & Todd, B. (2018). Challenges in Nanofluidics—Beyond Navier–Stokes at the Molecular Scale. Processes, 6, 144-157.

Fang, T., Wang, M., Gao, Y., Zhang, Y., Yan, Y., & Zhang, J. (2019). Enhanced Oil Recovery with CO_2/N_2 Slug in Low Permeability Reservoir: Molecular Dynamics Simulation. Chemical Engineering Science, 197, 204-211.

Hansen, J. S., Todd, B. D., & Daivis, P. J. (2011). Prediction of Fluid Velocity Slip at Solid Surfaces. Physical Review E: Statistical Nonlinear Soft Matter Physical, 84, 016313.

Hess, B. (2002). Determining the Shear Viscosity of Model Liquids from Molecular Dynamics Simulations. The Journal of Chemical Physics, 116.

Hoover, W. G., & Hoover, C. G. (2005). Nonequilibrium Molecular Dynamics. Condensed Matter Physics, 8, 247-260.

Ichikawa, Y., Kawamura, K., Fujii, N., & Nattavut, T. (2002). Molecular Dynamics and Multiscale Homogenization Analysis of Seepage/Diffusion Problem in Bentonite Clay. International Journal for Numerical Methods in Engineering, 54, 1717-1749.

Kannam, S. K., Todd, B. D., Hansen, J. S., & Daivis, P. J. (2013). How Fast Does Water Flow in Carbon Nanotubes? Journal of Chemical Physics, 138, 094701.

Katsumi, T., Onikata, M., Hasegawa, S., Lin, L.-C., Kondo, M., & Kamon, M. (2015). Chemical Compatibility of Modified Bentonite Permeated with Inorganic Chemical Solutions. In Yong, R. N., & Thomas, H. R. (Ed.), The third conference organized by the British Geotechnical Association and Cardiff School of Engineering, Cardiff University, (pp. 419-424). Edinburgh, UK.

Krisnanto, S., & Rahardjo, H. (2018). Advancement in the Analysis of Seepage through Cracked Soils. Journal of Engineering and Technological Sciences, 50, 566-577.

Liu, B., Qi, C., Zhao, X., Teng, G., Zhao, L., Zheng, H., Zhan, K., & Shi, J. (2018). Nanoscale Two-Phase Flow of Methane and Water in Shale Inorganic Matrix. The Journal of Physical Chemistry C, 122, 26671-26679.

Li, Y.-C., Wei, S.-J., Xu, N., & He, Y. (2020). Internal Forces within the Layered Structure of Na-Montmorillonite Hydrates: Molecular Dynamics Simulation. The Journal of Physical Chemistry C, 124, 25557-25567.

Mitchell, J. K., & Soga, K. (2005). Fundamentals of Soil Behavior. New Jersey: John Wiley & Sons, Inc.

Plimpton, S. (1995). Fast Parallel Algorithms for Short-Range Molecular Dynamics. Journal of Computational Physics, 117, 1-19.

Ramos-Alvarado, B., Kumar, S., & Peterson, G. P. (2016). Hydrodynamic Slip in Silicon Nanochannels. Physical Review E, 93, 033117.

Sam, A., Hartkamp, R., Kumar Kannam, S., Babu, J. S., Sathian, S. P., Daivis, P. J., & Todd, B. D. (2020). Fast Transport of Water in Carbon Nanotubes: A Review of Current Accomplishments and Challenges. Molecular Simulation, 1-20.

Shackelford, C. D. (2005). Environmental Issues in Geotechnical Engineering. In the 16th International Conference on Soil Mechanics and Geotechnical Engineering, (pp. 95-122). Millpress Science Publishers.

Simonnin, P., Marry, V., Noetinger, B., Nieto-Draghi, C., & Rotenberg, B. (2018). Mineral- and Ion-Specific Effects at Clay–Water Interfaces: Structure, Diffusion, and Hydrodynamics. The Journal of Physical Chemistry C, 122, 18484-18492.

Stukowski, A. (2010). Visualization and Analysis of Atomistic Simulation Data with Ovito–the Open Visualization Tool. Modelling and Simulation in Materials Science and Engineering, 18.

Travis, K. P., Todd, B. D., & Evans, D. J. (1997). Departure from Navier-Stokes Hydrodynamics in Confined Liquids. Physical Review E, 55, 4288-4295.

Yeh, I.-C., & Hummer, G. (2004). System-Size Dependence of Diffusion Coefficients and Viscosities from Molecular Dynamics Simulations with Periodic Boundary Conditions. The Journal of Physical Chemistry B, 15873-15879.

Yin, Y.-M., & Zhao, L.-L. (2020). Effects of Salt Concentrations and Pore Surface Structure on the Water Flow through Rock Nanopores. Acta Physica Sinica, 69.